


Cite this: *Dalton Trans.*, 2019, **48**, 4176

Heterobimetallic ruthenium–zinc complexes with bulky N-heterocyclic carbenes: syntheses, structures and reactivity†

Maialen Espinal-Viguri, Victor Varela-Izquierdo, Fedor M. Miloserdov, Ian M. Riddlestone, Mary F. Mahon* and Michael K. Whittlesey *

The ruthenium–zinc heterobimetallic complexes, $[\text{Ru}(\text{IPr})_2(\text{CO})\text{ZnMe}][\text{BAR}^{\text{F}}_4]$ (**7**), $[\text{Ru}(\text{IBiox6})_2(\text{CO})(\text{THF})\text{ZnMe}][\text{BAR}^{\text{F}}_4]$ (**12**) and $[\text{Ru}(\text{IMes})(\text{PPh}_3)(\text{CO})\text{ZnMe}]$ (**15**), have been prepared by reaction of ZnMe_2 with the ruthenium N-heterocyclic carbene complexes $[\text{Ru}(\text{IPr})_2(\text{CO})\text{H}][\text{BAR}^{\text{F}}_4]$ (**1**), $[\text{Ru}(\text{IBiox6})_2(\text{CO})(\text{THF})\text{H}][\text{BAR}^{\text{F}}_4]$ (**11**) and $[\text{Ru}(\text{IMes})(\text{PPh}_3)(\text{CO})\text{HCl}]$ respectively. **7** shows clean reactivity towards H_2 , yielding $[\text{Ru}(\text{IPr})_2(\text{CO})(\eta^2\text{-H}_2)(\text{H})_2\text{ZnMe}][\text{BAR}^{\text{F}}_4]$ (**8**), which undergoes loss of the coordinated dihydrogen ligand upon application of vacuum to form $[\text{Ru}(\text{IPr})_2(\text{CO})(\text{H})_2\text{ZnMe}][\text{BAR}^{\text{F}}_4]$ (**9**). In contrast, addition of H_2 to **12** gave only a mixture of products. The tetramethyl IBiox complex $[\text{Ru}(\text{IBioxMe}_4)_2(\text{CO})(\text{THF})\text{H}][\text{BAR}^{\text{F}}_4]$ (**14**) failed to give any isolable Ru–Zn containing species upon reaction with ZnMe_2 . The cyclometallated NHC complex $[\text{Ru}(\text{IMes})(\text{PPh}_3)(\text{CO})\text{ZnMe}]$ (**15**) added H_2 across the Ru–Zn bond both in solution and in the solid-state to afford $[\text{Ru}(\text{IMes})(\text{PPh}_3)(\text{CO})(\text{H})_2\text{ZnMe}]$ (**17**), with retention of the cyclometallation.

Received 20th December 2018,

Accepted 19th February 2019

DOI: 10.1039/c8dt05023f

rsc.li/dalton

Introduction

Heterobimetallic complexes featuring a transition metal (TM) in partnership with a Lewis acidic (LA), typically main group element, have been the focus of considerable interest¹ because of their potential to bring about the cooperative activation of E–H (E = H, N, Si *etc.*) bonds.² The most commonly found heterobimetallic complexes feature a late transition metal (groups 8–10) and an element from group 13 (particularly B and Al) and, in many cases, are readily prepared by salt elimination reaction of a TM anion with a halide of the LA.³ While this approach is very flexible in that there are many possible TM and LA fragments that can be combined in this way, one (if not both) of the partners is typically left coordinatively saturated, reducing the subsequent reactivity for bond activation processes. An alternative approach which has been employed, although less frequently, is an alkane elimination pathway *via* the reaction of a TM hydride precursor with a LA hydrocarbyl reagent.⁴ This synthetic approach does come with potential issues (*e.g.* the use of highly pyrophoric group 13 trialkyls, cost of Ga/InMe₃ *etc.*), but does allow access to heterobimetallic

complexes with unsaturation at both centres, thereby opening up an opportunity to probe true TM–LA cooperativity.

Very recently, we reported that addition of GaMe₃, InMe₃ and ZnEt₂ to the bulky N-heterocyclic carbene (NHC) stabilised cationic ruthenium hydride complex $[\text{Ru}(\text{IPr})_2(\text{CO})\text{H}][\text{BAR}^{\text{F}}_4]$ (**1**; IPr = 1,3-bis(2,6-diisopropylphenyl)imidazol-2-ylidene; $\text{BAR}^{\text{F}}_4 = [\text{B}\{\text{C}_6\text{H}_3(3,5\text{-CF}_3)_2\}_4]^-$)⁵ resulted in alkane elimination and formation of the Ru–Ga, Ru–In and Ru–Zn complexes **2–4** shown in Scheme 1.⁶ Of most relevance to this current paper was the ruthenium–zinc complex $[\text{Ru}(\text{IPr})_2(\text{CO})\text{ZnEt}][\text{BAR}^{\text{F}}_4]$ (**4**) which, upon treatment with H_2 , both coordinated dihydrogen at Ru and added H_2 across the Ru–Zn bond to give $[\text{Ru}(\text{IPr})_2(\text{CO})(\eta^2\text{-H}_2)(\text{H})_2\text{ZnEt}][\text{BAR}^{\text{F}}_4]$ (**5**). Dissociation of the dihydrogen ligand from this highly fluxional species took place upon heating under vacuum to give the agostically stabilised dihydride complex, $[\text{Ru}(\text{IPr})_2(\text{CO})(\text{H})_2\text{ZnEt}][\text{BAR}^{\text{F}}_4]$ (**6**, Scheme 1).^{7,8}

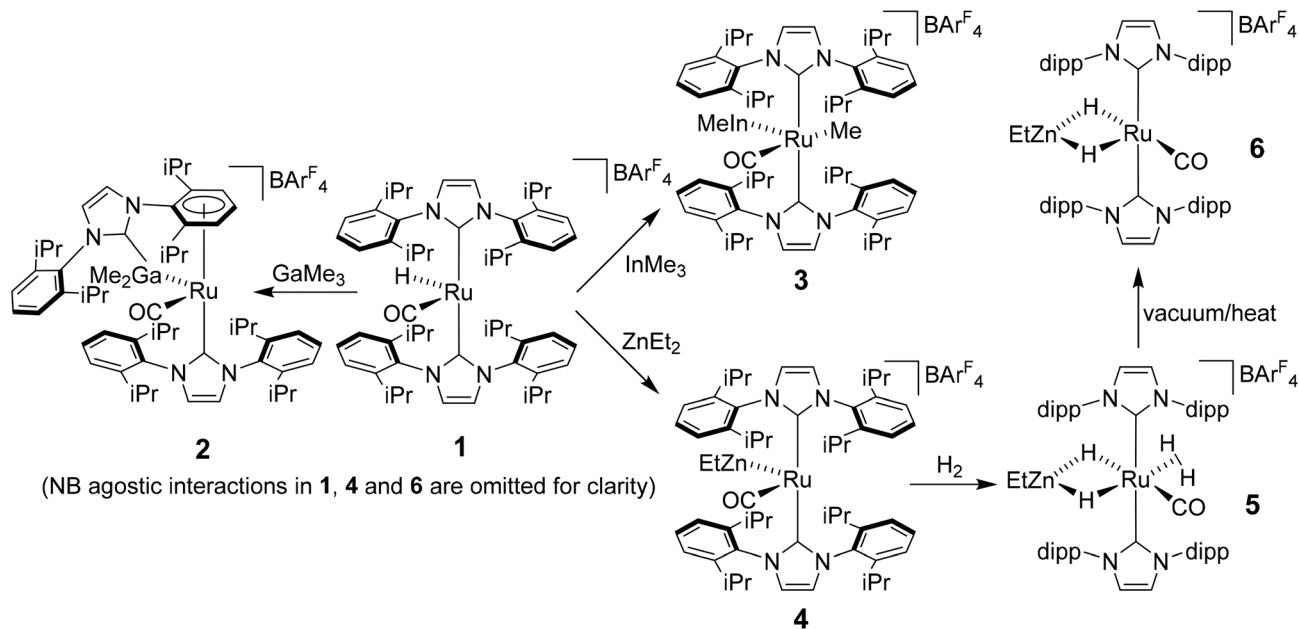
Structural analysis showed that **4** (as well as **1**) was also agostically stabilised, in this case through a bifurcated $\eta^3\text{-H}_2\text{C}$ ξ -agostic interaction involving an ¹Pr substituent of the IPr ligand. Thus, while **1** and **4** appear at first sight to be rare examples of isolable, four-coordinate Ru(II) complexes, the bifurcated agostic interactions impart formally 18-electron configurations. The participation of the bulky IPr ligand in forming agostic interactions seems to play a role in allowing **1**, **4** and **6** to be isolated and structurally characterised, given that the less sterically crowded analogue $[\text{Ru}(\text{IMes})_2(\text{CO})\text{H}]^+$ (IMes = 1,3-bis(2,4,6-trimethylphenyl)imidazol-2-ylidene) is found only as an oil.⁹

Department of Chemistry, University of Bath, Claverton Down, Bath BA2 7AY, UK.

E-mail: m.k.whittlesey@bath.ac.uk

† Electronic supplementary information (ESI) available: CCDC 1882150–1882159. For ESI and crystallographic data in CIF or other electronic format see DOI: 10.1039/c8dt05023f





Scheme 1 Summary of the reactivity of $[\text{Ru}(\text{IPr})_2(\text{CO})\text{H}][\text{BARF}_4]$ (**1**) with ZnEt_2 and MMe_3 ($\text{M} = \text{Ga}, \text{In}$).

Herein, we describe efforts to elaborate on the chemistry of **1** and **4–6** through studies in which (i) the reactivity of **1** towards other ZnR_2 reagents ($\text{R} = \text{Me}, \text{Ph}$) is probed and (ii) analogues containing the bulky oxazoline-derived IBiox class of NHC ligands are investigated. We also show that the formation of coordinatively unsaturated and reactive (NHC)Ru–Zn complexes is not limited to just cationic Ru–H precursors.¹⁰

Results and discussion

Reactivity of **1** towards ZnR_2 reagents

The methyl zinc analogue of **4**, $[\text{Ru}(\text{IPr})_2(\text{CO})\text{ZnMe}][\text{BARF}_4]$ (**7**), was prepared by subjecting a $\text{C}_6\text{H}_5\text{F}$ solution of **1** to a slight excess of a toluene solution of ZnMe_2 . **7** was isolated as a dark red solid in good yield (73%) and exhibited diagnostic low frequency ^1H ($\delta - 0.86$) and ^{13}C ($\delta - 0.7$) NMR resonances for the Zn–Me group, along with high frequency ^{13}C signals ($\delta 200.6$ and 188.0) arising from the presence of the carbenic and carbonyl carbons respectively. The structure of **7** was confirmed by X-ray crystallography (Fig. 1), which revealed a Ru–Zn distance of $2.3997(8)$ Å, comparable to that in **4** ($2.4069(7)$ Å). There was no reaction between **1** and ZnPh_2 (even upon heating to 70 °C) presumably due to the unfavourable combination of bulky substituents on the NHC and Zn.

Upon exposure of a fluorobenzene solution of **7** to 1 atm H_2 , an instantaneous change in colour from red-orange to colourless was observed, resulting from the formation of the dihydrogen dihydride complex, $[\text{Ru}(\text{IPr})_2(\text{CO})(\eta^2\text{-H}_2)(\text{H})_2\text{ZnMe}][\text{BARF}_4]$ (**8**, Scheme 2).¹¹ This showed less fluxional behavior than the ZnEt analogue **5**, exhibiting three low frequency hydride signals ($\delta -5.15, -7.83$ and -12.16 in a 2 : 1 : 1 ratio) at room temperature compared to just two resonances for **5**

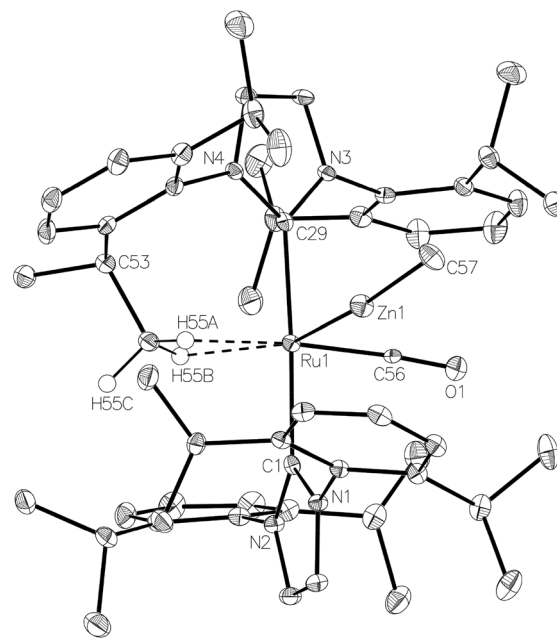
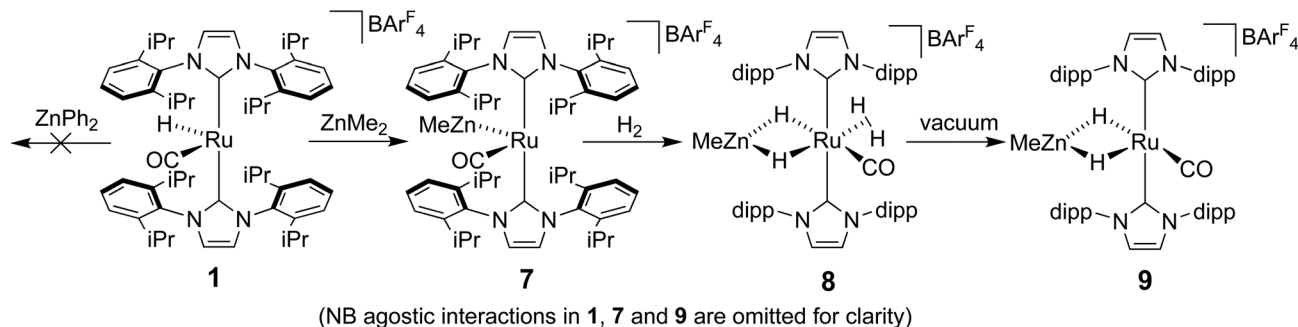


Fig. 1 Molecular structure of the cation in $[\text{Ru}(\text{IPr})_2(\text{CO})\text{ZnMe}][\text{BARF}_4]$ (**7**). Ellipsoids are shown at 30% probability. All hydrogen atoms (with the exception of those attached to C55) removed for clarity. Selected bond lengths (Å) and angles (°): Ru(1)–Zn(1) $2.3997(8)$, Ru(1)–C(1) $2.123(5)$, Ru(1)–C(29) $2.108(5)$, Ru(1)–C(56) $1.837(6)$, C(1)–Ru(1)–C(29) $175.4(2)$, C(56)–Ru(1)–Zn(1) $77.1(2)$.

($\delta -5.33$ and -12.13 in a 3 : 1 ratio). Cooling a THF solution of **8** to 238 K led to sharpening of the two lower frequency resonances, whereas that at *ca.* -5 ppm remained broader than the others even down to 218 K. Based upon the comparable chemical shifts and assignments in **5**, the three signals were



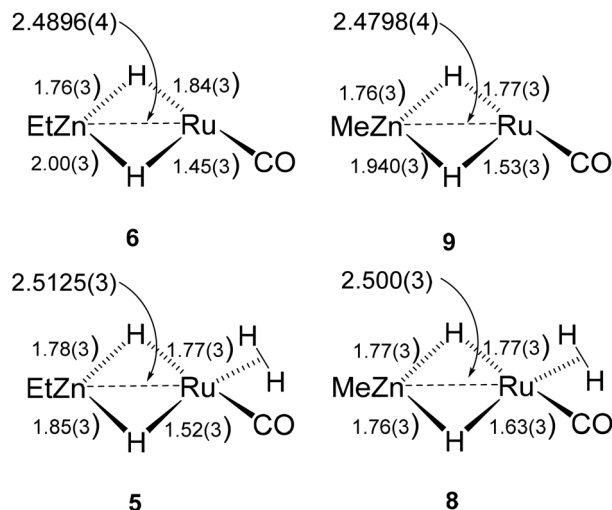


Scheme 2 Synthesis and reactivity of $[\text{Ru}(\text{IPr})_2(\text{CO})\text{ZnMe}][\text{BARF}_4]$ (7).

assigned to $\text{Ru}(\eta^2\text{-H}_2)$, Ru–H–Zn trans to CO and Ru–H–Zn trans to $\eta^2\text{-H}_2$ in order of decreasing frequency.

The $\eta^2\text{-H}_2$ ligand in 8 could be removed simply by the application of vacuum to a solid sample of the compound (*cf.* vacuum and heat for 5, Scheme 1). The resulting product, $[\text{Ru}(\text{IPr})_2(\text{CO})(\text{H})_2\text{ZnMe}][\text{BARF}_4]$ (9), was identified by the appearance of a low frequency ($\delta -25.77$) doublet ($^2J_{\text{HH}} = 7.7$ Hz) resonance for Ru–H–Zn trans to the agostic $\text{Ru}\cdots\text{H}_2\text{C}$ the IPr ligand (*vide infra*), together with a higher frequency doublet ($\delta -4.19$, $^2J_{\text{HH}} = 7.7$ Hz) arising from the Ru–H–Zn hydride trans to CO.

The Ru–Zn complexes 8 and 9 were characterised crystallographically (Fig. 2). As anticipated, a comparison of these two complexes to their ZnEt analogues 5 and 6 (Scheme 3) shows the same patterns *i.e.* elongation of the $\text{Ru}\cdots\text{Zn}$ distance relative to 4 and 7, less asymmetry of the Ru–H–Zn distances for H trans to CO and greater association with Ru for H trans to either an agostic interaction (6 and 9) or a dihydrogen ligand (5 and 8).



Scheme 3 Summary of key distances in $[\text{Ru}(\text{IPr})_2(\text{CO})(\text{H})_2\text{ZnR}][\text{BARF}_4]$ and $[\text{Ru}(\text{IPr})_2(\text{CO})(\eta^2\text{-H}_2)(\text{H})_2\text{ZnR}][\text{BARF}_4]$ (R = Et, Me).

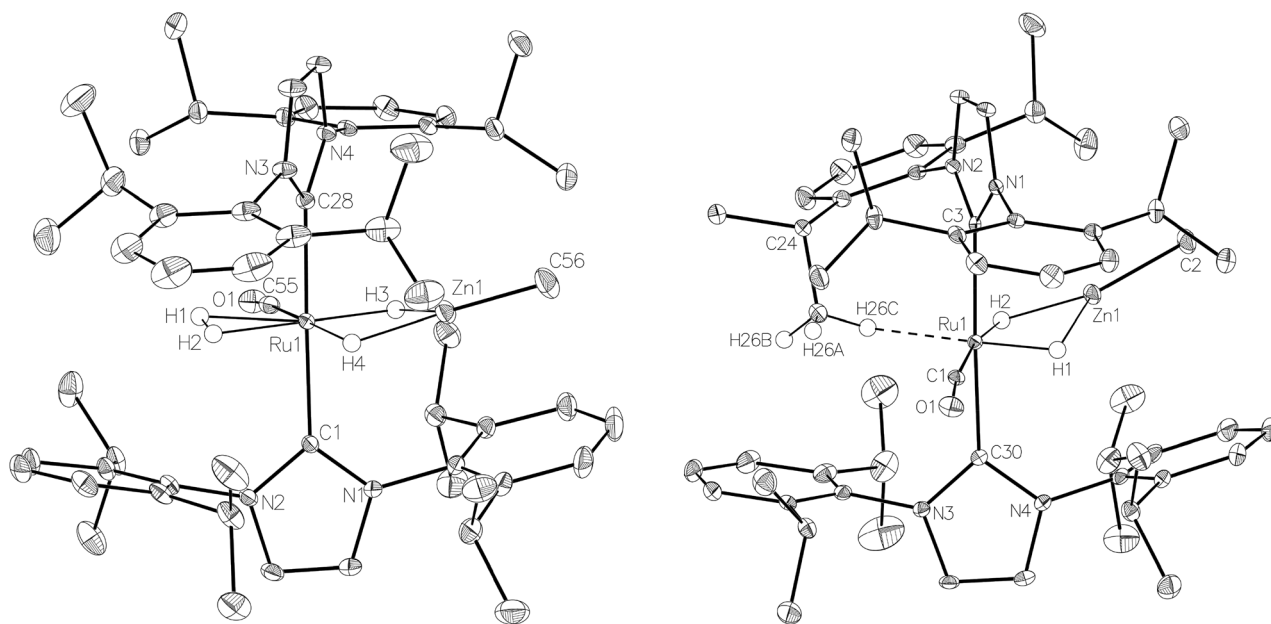


Fig. 2 Molecular structures of the cations in (left) $[\text{Ru}(\text{IPr})_2(\text{CO})(\eta^2\text{-H}_2)(\text{H})_2\text{ZnMe}][\text{BARF}_4]$ (8) and $[\text{Ru}(\text{IPr})_2(\text{CO})(\text{H})_2\text{ZnMe}][\text{BARF}_4]$ (right) (9). Ellipsoids are shown at 30% probability with all hydrogen atoms (except hydrides, those agostically bonded and the tentatively assigned dihydrogen ligand) removed for clarity.



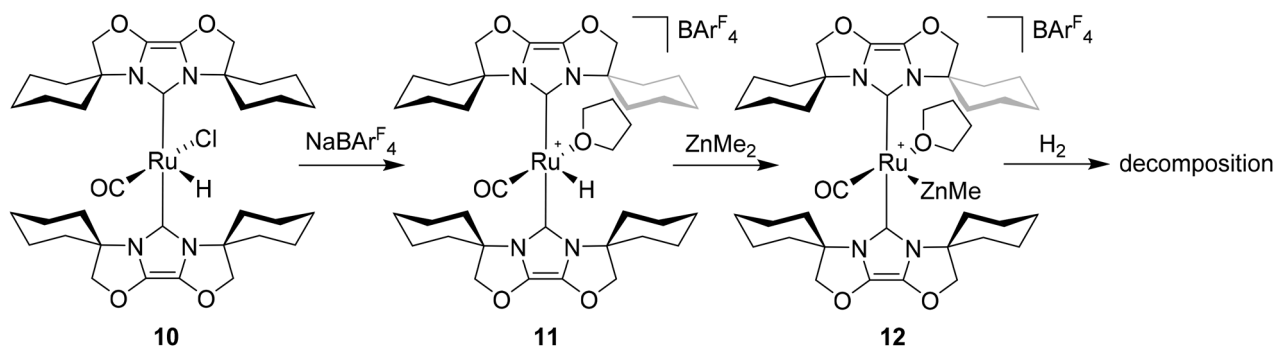
Synthesis and reactivity of Ru(IIbiox) complexes

Given the success of IPr in allowing access to isolable $[\text{Ru}(\text{NHC})_2(\text{CO})\text{H}]^+$ and $[\text{Ru}(\text{NHC})_2(\text{CO})\text{ZnR}]^+$ species, we turned our attention to the IBiox class of NHCs introduced by Glorius,¹² on the basis that they are also known to be sterically demanding and flexibly restricted. Moreover, in spite of their use for the preparation of low-coordinate Rh and Ir complexes,¹³ we were aware of just a single example of a Ru-IBiox complex at the outset of our work.¹⁴

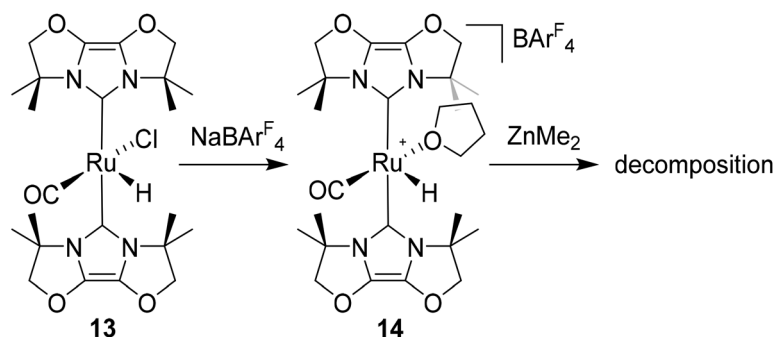
Employing previous methodology,¹⁵ the bis-carbene complexes $[\text{Ru}(\text{IBiox6})_2(\text{CO})\text{HCl}]$ (**10**; for structure of IBiox6, see Scheme 4) and $[\text{Ru}(\text{IBioxMe}_4)_2(\text{CO})\text{HCl}]$ (**13**; for structure of IBioxMe₄, see Scheme 5) were isolated in *ca.* 50–70% yield after heating $[\text{Ru}(\text{AsPh}_3)_3(\text{CO})\text{H}_2]$ with 2.5 equivalents of the free carbenes, followed by addition of dichloromethane. The ¹H NMR spectra of these 16-electron species displayed a low frequency hydride resonance (**10**: δ –24.75; **13**: δ –25.14) characteristic of $[\text{Ru}(\text{NHC})_2(\text{CO})\text{HCl}]$ complexes.^{15,16} Addition of $\text{NaBAR}^{\text{F}_4}$ led to abstraction of the chloride ligand to give $[\text{Ru}(\text{IBiox6})_2(\text{CO})(\text{THF})\text{H}][\text{BAR}^{\text{F}_4}]$ (**11**, Scheme 4) and $[\text{Ru}(\text{IBioxMe}_4)_2(\text{CO})(\text{THF})\text{H}][\text{BAR}^{\text{F}_4}]$ (**14**, Scheme 5) respectively. The X-ray structures of neither **11** nor **14** (Fig. 3) showed any agostic interactions to the substituents on the IBiox ligands (*e.g.* shortest C–H...Ru in **11** is 3.182 Å).^{13a,c} In order to relieve the electron-deficiency of the Ru(II) centres, a THF ligand resides in the metal coordination sphere of each complex *trans* to CO.¹⁷

The X-ray crystal structure of **10** and **13**, along with those of the cations in **11** and **14**, are shown in Fig. 3. A listing of metrical data for the compounds is given in Table 1. As expected, all four compounds exhibited square pyramidal geometries with the hydride ligand in an apical position. Analysis of the NHC tilting angle $\theta_{\text{NHC}}(\text{Ru}-\text{C}_{\text{NHC}}-\text{centroid}_{\text{NHC}})$ ¹⁸ revealed angles of $>170^\circ$ in all cases, showing that, despite the coordinative unsaturation at ruthenium, the IBiox ligands remain free of any structural distortions akin to those seen in some $[\text{M}(\text{IBiox})_3]^+$ (M = Rh, Ir) species.^{13c}

Efforts to generate new Ru–Zn containing complexes through reaction of **11** and **14** with ZnMe_2 was successful only in the case of the former,¹⁹ which generated $[\text{Ru}(\text{IBiox6})_2(\text{CO})(\text{THF})\text{ZnMe}][\text{BAR}^{\text{F}_4}]$ (**12**, Fig. 4 and Scheme 4). A comparison between the structures of **4** and **12** yield some superficial similarities and some interesting differences. Both structures contain two *trans* NHC ligands and coordination bonds in the equatorial plane of which two are common, namely, one to a zinc centre and one to a CO ligand. In **4**, the remaining site is occupied by a bifurcated agostic interaction, while in **12**, there is coordination of a THF molecule. In gross terms, the structures of both cations overlay reasonably well, but the biggest significant difference between them lies in the relative orientations of the NHC ligands. In **4**, the angle between the mean planes based on the 5-membered NHC rings is relatively staggered at 102° , while the comparable angle in **12** (32°) reflects a more eclipsed carbene conformation. The arising steric ramifications are that the $\text{C}_{\text{NHC}}-\text{Ru}-\text{C}_{\text{NHC}}$ angle of $177.32(19)^\circ$ in **4**



Scheme 4 Synthesis and reactivity of Ru(IIbiox6) complexes.



Scheme 5 Synthesis and reactivity of Ru(IIbioxMe₄) complexes.



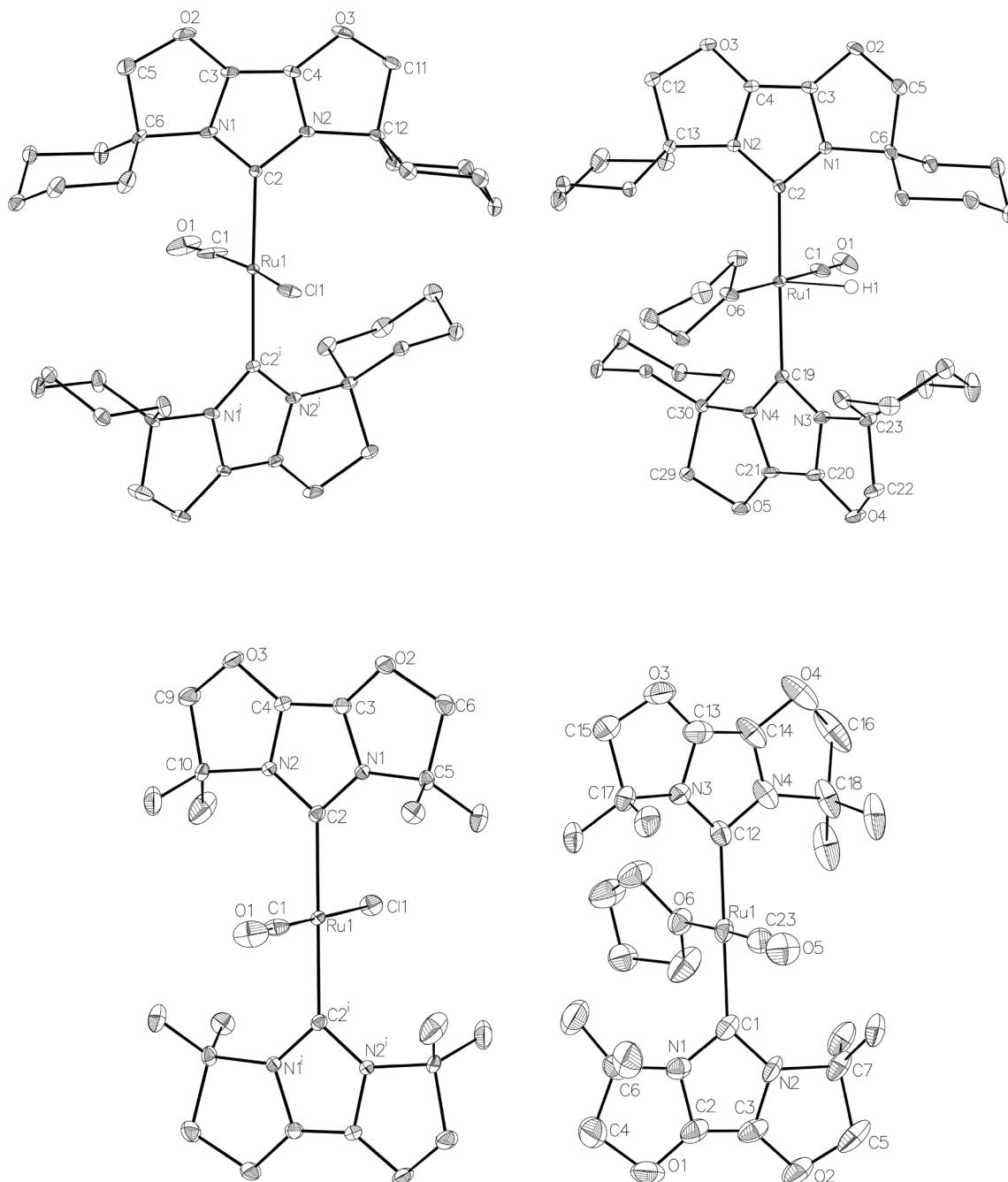


Fig. 3 Molecular structures of [Ru(1BIox6)₂(CO)HCl] (**10**, top left), [Ru(1BIoxMe₄)₂(CO)HCl] (**13**, bottom left) and the cations in [Ru(1BIox6)₂(CO)(THF)H][BARF₄] (**11**, top right) and [Ru(1BIoxMe₄)₂(CO)(THF)H][BARF₄] (**14**, bottom right). In all cases, ellipsoids are represented at 30% probability. In **10**, solvent hydrogen atoms and disorder have been omitted for clarity. Symmetry operation: $^i1 - x, y, \frac{1}{2} - z$. In **11**, hydrogen atoms, with the exception of the hydride ligand, are omitted for clarity. Only one disordered component of the hydride ligand and of C22 is illustrated. In **13**, disorder has been omitted for clarity. Symmetry operation: $^i1 - x, 1 - y, 1 - z$. In **14**, disorder was rampant and only one component is illustrated, for clarity.

is noticeably more linear than the $170.96(10)^\circ$ angle observed in **12**. It is possible that the significantly shorter Ru–Zn distance of $2.3819(4)$ Å in **12** (*cf.* $2.4069(7)$ Å in **4**) may reflect the less encumbered access of the zinc ligand, towards the ruthenium centre, *via* the opposite face of the cation to the NHC ligand fold.

Upon exposure to either 1 or 5 atm H₂, NMR spectra of fluorobenzene solutions of **12** exhibited signals for free 1BIox6

as well as the salt [1BIox6-H][BARF₄]. Any products of initial reaction with H₂ therefore appear to be of only limited stability.

Ru–Zn bond formation from a neutral Ru–H precursor

The premise behind the initial synthesis of **1** was that addition of ZnR₂ to an electrophilic ruthenium hydride complex would



Table 1 Selected bond lengths (Å) and angles (°) in Ru(IIbiox) complexes 10–14

	$[Ru(IIbiox)_2(CO)HCl]$		$[Ru(IIbiox)_2(CO)(THF)X]^+$		
	10	13	11 (X = H)	14 (X = H)	12 (X = ZnMe)
Ru–C _{IBiox}	2.122(4)	2.086(3)	2.112(2), 2.116(3)	2.093(3), 2.098(3)	2.120(3), 2.127(3)
Ru–CO	1.782(19)	1.825(11)	1.797(4)	1.795(4)	1.818(3)
Ru–Cl	2.375(4)	2.405(3)	—	—	—
Ru–O	—	—	2.168(2)	2.197(2)	—
Ru–Zn	—	—	—	—	2.3819(4)
Ru–C _{IBiox} –IBiox _{centroid} ¹⁸	175.87	176.96	174.07, 174.01	N/A due to disorder	170.84, 171.13
Cl–Ru–CO	170.0(8)	179.2(5)	—	—	—
O–Ru–CO	—	—	178.89(17)	177.99(13)	154.59(10)
Zn–Ru–CO	—	—	—	—	134.11(6)

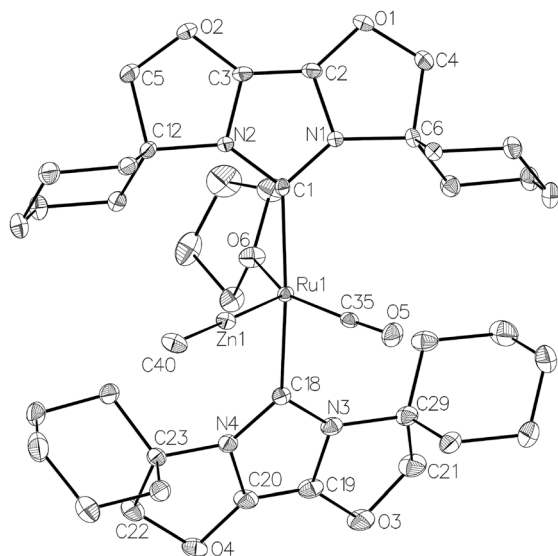
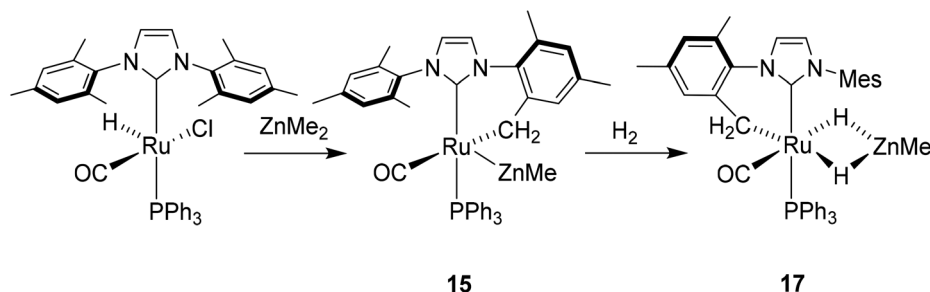


Fig. 4 Molecular structure of the cation in $[Ru(IIbiox)_6(CO)(THF)ZnMe][BARF_4]$ (**12**). Ellipsoids are shown at 30% probability. Only one component arising from the disordered carbons (C37 and C38) in the THF ligand is illustrated.

result in the facile elimination of an alkane and formation of a new Ru–Zn containing species. In an effort to test whether a cationic (NHC)Ru hydride precursor was necessary, we examined the reaction of the neutral precursor $[Ru(IMes)(PPh_3)(CO)]$

HCl] with $ZnMe_2$. In the presence of 5 equiv. $ZnMe_2$, a rapid reaction ensued to form the cyclometallated complex $[Ru(IMes)(PPh_3)(CO)ZnMe]$ (**15**, Scheme 6) as determined by 1H and $^{31}P\{^1H\}$ NMR spectroscopy. The formation of **15** was accompanied by small amounts of a second product (assigned tentatively as the non-metallated ruthenium chloride complex, $[Ru(IMes)(PPh_3)(CO)(ZnMe)Cl]$ (**16**; see ESI[†])), the concentration of which correlated with the rate of addition of $ZnMe_2$. **15** was itself present as major (**15a**) and minor (**15b**) forms in solution. As a result, the Ru–CH₂ group arising from C–H activation of the IMes ligand gave rise to two sets of diastereotopic signals in the proton NMR spectrum; in $THF-d_8$, **15a** showed a broad triplet ($^2J_{HH} = ^3J_{HP} = 5.6$ Hz) at δ 2.61 and a doublet of doublets ($^3J_{HP} = 11.6$ Hz, $^2J_{HH} = 6.7$ Hz) at δ 0.98 (each of integral 1, which both correlated (1H – ^{13}C HSQC) to a methylene carbon resonance at δ 31), while **15b** displayed a multiplet at δ 1.52 and a doublet of doublets ($^3J_{HP} = 14.4$ Hz, $^2J_{HH} = 8.6$ Hz) at δ 1.40; both resonances correlated to a ^{13}C NMR signal at δ 32.²⁰

The similarity of chemical shifts and J values for both species (*e.g.* each exhibited a high frequency resonance for the carbenic carbon with a $^2J_{CP}$ value of >80 Hz, indicative of a *trans* IMes–Ru–PPh₃ geometry) suggested that they were most likely conformers. There was a slight solvent dependence on the solution ratio of **15a** : **15b** (88 : 12 and 82 : 18 in C_6D_6 and $THF-d_8$ respectively). The two species were shown to be in exchange in $THF-d_8$ by EXSY, although NOESY measurements failed to divulge any information as to the spatial difference between **15a** and **15b**. We were unable to establish any difference



Scheme 6 Formation of $[Ru(IMes)(PPh_3)(CO)ZnMe]$ (**15**) and $[Ru(IMes)(PPh_3)(CO)(H)_2ZnMe]$ (**17**).



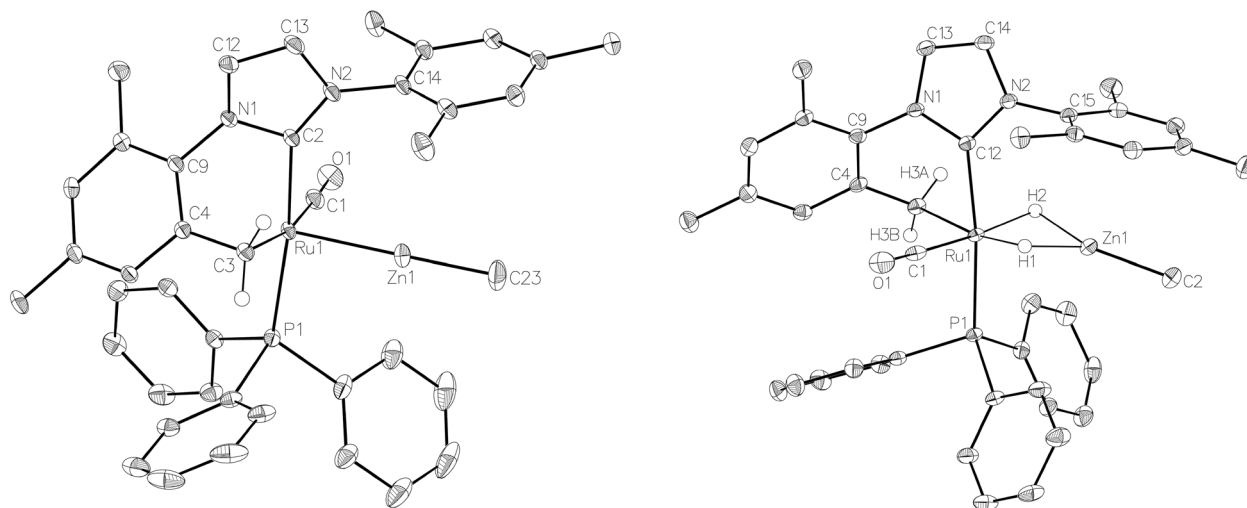


Fig. 5 Molecular structures of (left) $[\text{Ru}(\text{IMes})(\text{PPh}_3)(\text{CO})\text{ZnMe}]$ (**15**) and (right) $[\text{Ru}(\text{IMes})(\text{PPh}_3)(\text{CO})(\text{H})_2\text{ZnMe}]$ (**17**). Ellipsoids are shown at 30% probability with all hydrogen atoms (except Ru–CH₂ and Ru–H) removed for clarity. Selected bond lengths (Å) and angles (°) in **15**: Ru(1)–C(1) 1.857(2), Ru(1)–C(2) 2.071(2), Ru(1)–C(3) 2.224(2), Ru(1)–P(1) 2.3360(5), Ru(1)–Zn(1) 2.3677(3), C(2)–Ru(1)–P(1) 172.32(6), C(1)–Ru(1)–C(3) 169.63(9), Ru(1)–C(3)–C(4) 83.39(12). **17**: Ru(1)–C(1) 1.874(2), Ru(1)–C(12) 1.946(2), Ru(1)–C(3) 2.1971(19), Ru(1)–P(1) 2.3342(5), Ru(1)–Zn(1) 2.4828(3), C(12)–Ru(1)–P(1) 169.10(6), C(1)–Ru(1)–C(3) 98.77(8), Ru(1)–C(3)–C(4) 108.65(13).

crystallographically as measurements of a number of different single crystals only ever afforded the same structure as shown in Fig. 5.

Upon addition of 1 atm H₂ to a deep red-orange C₆D₆ solution of **15**, an instant colour change to very pale ensued from formation of $[\text{Ru}(\text{IMes})(\text{PPh}_3)(\text{CO})(\text{H})_2\text{ZnMe}]$ (**17**). The ¹H NMR spectrum showed the presence of two doublet hydride resonances at δ –6.77 (²J_{HP} = 14.9 Hz) and δ –9.19 (²J_{HP} = 5.0 Hz), alongside a higher frequency doublet at δ 3.22 and doublet of doublets at δ 1.83, consistent with addition of H₂ across the Ru–Zn bond rather than reversal of the IMes cyclometallation. This irreversibility contrasts with what we observed previously in the case of the related cyclometallated hydride derivative $[\text{Ru}(\text{IMes})(\text{PPh}_3)_2(\text{CO})\text{H}]$, which reacted with H₂ to form $[\text{Ru}(\text{IMes})(\text{PPh}_3)_2(\text{CO})\text{H}_2]$.^{20a} Equally surprisingly, monitoring of the reaction with H₂ in the solid-state by IR spectroscopy showed complete depletion of ν_{CO} for **15** at 1860 cm^{–1} and appearance of a new carbonyl absorption band at 1941 cm^{–1} for **17** upon stirring a ground up microcrystalline sample of the former under 1 atm H₂ for 2 days at room temperature.

The X-ray crystal structures of **15** and **17** (Fig. 5) show clearly the transformation of 5-coordinate **15** to six-coordinate **17** upon reaction with H₂. As anticipated (*vide supra*), elongation of the Ru–Zn distance from 2.3677(3) Å to 2.4828(3) Å takes place upon H₂ addition. Both bridging hydrogens were located and refined without restraints. As in **6** and **9**, the hydride *trans* to CO was more evenly shared between Ru and Zn than that, which in the case of **17**, lies *trans* to the methylene group of the activated IMes ligand. As a result of cyclometallation, neither **15** nor **17** showed a strictly linear C_{IMes}–Ru–P geometry (172.32(6) and 169.10(6)° respectively). **15** exhibited a particularly noticeable distortion of the angle at the cyclometallated methylene carbon (Ru(1)–C(3)–C(4) = 83.39(12)°).²¹

Preliminary studies to investigate the mechanism of formation of **17** revealed that exposure of **17** to D₂ (1 atm) resulted in slow (1 day, room temperature) deuterium incorporation into both Ru–H–Zn positions, but no H/D exchange at RuCH₂. This excludes exchange taking place *via* a reversible reductive elimination pathway involving both RuH and RuCH₂.²² The viability of an alternative pathway through phosphine dissociation was probed by reaction of **17** with 5 equiv. P(*p*-tolyl)₃. Slow PPh₃/P(*p*-tolyl)₃ was indeed observed, but the relevance of this to the H/D exchange was complicated by the appearance of other low frequency proton signals arising from the decomposition of **17** that can be seen in solution over 1–2 days.

Conclusions

We have reported that ZnMe₂ reacts with both cationic and neutral ruthenium hydride precursors containing bulky N-heterocyclic carbene ligands to afford new heterobimetallic complexes containing Ru–Zn bonds. The IPr complex $[\text{Ru}(\text{IPr})_2(\text{CO})\text{ZnMe}][\text{BAR}^{\text{F}}_4]$ (**7**) proved to be similar in terms of both structure and reactivity towards H₂ to the previously reported ZnEt derivative **4**. Use of the bulky IBiox carbene ligands met with varying levels of success; the cyclohexyl substituted derivative IBiox6 gave $[\text{Ru}(\text{IBiox6})_2(\text{CO})(\text{THF})\text{ZnMe}][\text{BAR}^{\text{F}}_4]$ (**12**), whereas the analogous tetramethyl IBioxMe₄ derivative could not be isolated. Of particular interest was the formation of the neutral complex $[\text{Ru}(\text{IMes})(\text{PPh}_3)(\text{CO})\text{ZnMe}]$ (**15**), which added H₂ across the Ru–Zn bond whilst retaining the cyclometallated NHC ligand. As noted above, this behaviour contrasts with the reversal of cyclometallation that is brought about upon exposure of $[\text{Ru}(\text{IMes})(\text{PPh}_3)_2(\text{CO})\text{H}]$ to H₂.^{20a} This, together with the fact that **4** reacts with HBcat to



bring about dehydrocoupling (and generation of 5^{6b}) in contrast to **1** which reacts with HBeat with loss of H_2 and formation of the stable boryl complex $[Ru(IPr)_2(CO)Bcat][BAR^F_4]^{-}$,⁵ provides evidence for very different reactivity between Ru–Zn and Ru–H containing species. Indeed, efforts to probe the reactivity of **15** towards a broader range of E–H bonds, as well as prepare derivatives of the complex containing other metalated ligands, are in progress.

Experimental

All manipulations were carried out using standard Schlenk, high vacuum and glovebox techniques using dried and degassed solvents. NMR spectra were recorded on Bruker Avance 400 and 500 MHz NMR spectrometers and run either locked in CD_2Cl_2 (referenced to δ 5.32 (1H); 54.0 (^{13}C)), $CDCl_3$ (referenced to δ 7.26 (1H); 54.0 (^{13}C)), THF- d_8 (referenced to δ 3.58 (1H); 67.2 (^{13}C)) or C_6D_6 (referenced to δ 7.15 (1H); 128.0 (^{13}C)), or unlocked in C_6H_5F (1H NMR spectra referenced to the centre of the downfield multiplet at δ 7.11). IR spectra were recorded in solution (CH_2Cl_2 , CD_2Cl_2 , $CDCl_3$ or THF) or in KBr discs on a Nicolet Nexus spectrometer. Elemental analyses were performed by Elemental Microanalysis Ltd, Okehampton, Devon, UK. $[Ru(IPr)_2(CO)H][BAR^F_4]^{-}$ (**1**),⁵ IBiox6,^{12b} IBioxMe,⁴ and $[Ru(IMes)(PPh_3)(CO)HCl]^{23}$ were prepared according to the literature.

$[Ru(IPr)_2(CO)ZnMe][BAR^F_4]^{-}$ (**7**)

Addition of $ZnMe_2$ (25 μ L of 1.0 M in toluene, 0.025 mmol) to a solution of **1** (40 mg, 0.023 mmol) in C_6H_5F (0.6 mL) resulted in an instantaneous change in colour from yellow to deep red. The reaction mixture was layered with hexane, which gave dark red crystals of **7**. Yield 30 mg (73%). 1H NMR: δ_H (500 MHz, CD_2Cl_2 , 298 K) 7.73 (s, 8H, $[BAR^F_4]^{-}$), 7.56 (s, 4H, $[BAR^F_4]^{-}$), 7.51 (t, $J = 7.8$ Hz, 4H, Ar), 7.32 (dd, $J = 7.8, 1.4$ Hz, 4H, Ar), 7.27 (dd, $J = 7.8, 1.4$ Hz, 4H, Ar), 7.03 (s, 4H, NCH=NCH), 2.42 (sept, $^3J_{HH} = 6.8$ Hz, 4H, $CH(CH_3)_2$), 2.32 (sept, $^3J_{HH} = 6.8$ Hz, 4H, $CH(CH_3)_2$), 1.10 (d, $^3J_{HH} = 6.8$ Hz, 12H, $CH(CH_3)_2$), 1.07 (d, $^3J_{HH} = 6.8$ Hz, 12H, $CH(CH_3)_2$), 1.00 (d, $^3J_{HH} = 6.8$ Hz, 12H, $CH(CH_3)_2$), 0.65 (d, $^3J_{HH} = 6.8$ Hz, 12H, $CH(CH_3)_2$), -0.86 (s, 3H, $ZnCH_3$). $^{13}C\{^1H\}$ NMR: δ_C (101 MHz, CD_2Cl_2 , 298 K, $[BAR^F_4]^{-}$ signals are omitted) 200.6 (s, RuCO), 188.0 (s, Ru_{NHC}), 146.5 (s), 146.3 (s), 135.7 (s), 131.7 (s), 126.3 (s), 126.1 (s), 124.1 (s), 29.8 (s), 29.3 (s, $CH(CH_3)_2$), 25.9 (s), 24.7 (s), 24.2 (s), 23.7 (s, $CH(CH_3)_2$), -0.71 (s, $ZnCH_3$). IR (CH_2Cl_2 , cm^{-1}): 1919 (ν_{CO}). Anal. calcd for $C_{88}H_{87}BN_4OF_{24}ZnRu$: C, 57.14, H, 4.74, N, 3.03. Found: C, 56.79, H, 4.70, N, 2.78.

$[Ru(IPr)_2(CO)(\eta^2-H_2)(H)_2ZnMe][BAR^F_4]^{-}$ (**8**)

A J. Young's resealable NMR tube was charged with a C_6H_5F (0.6 mL) solution of **7** (35 mg, 0.020 mmol) and $ZnMe_2$ (22 μ L, 1.0 M in toluene, 0.022 mmol) added. The resulting red solution was evaporated to dryness, redissolved in C_6H_5F (0.3 mL), degassed (freeze–pump–thaw $\times 3$) and placed under 1 atm H_2 . The solution was layered with H_2 -purged hexane to afford pale-

colourless crystals of **8**. Yield 25 mg (69%). Material for elemental analysis was prepared by slow evaporation of a sample of **8** prepared *via* exposure of a CH_2Cl_2 solution of **7** to H_2 . 1H NMR: δ_H (500 MHz, CD_2Cl_2 , 298 K) 7.73 (s, 8H, $[BAR^F_4]^{-}$), 7.56 (s, 4H, $[BAR^F_4]^{-}$), 7.52 (t, $J = 8.0$ Hz, 4H, Ar), 7.28 (d, $J = 8.0$ Hz, 8H, Ar), 7.09 (s, 4H, NCH=NCH), 2.19 (sept, $^3J_{HH} = 6.8$ Hz, 8H, $CH(CH_3)_2$), 1.10 (d, $^3J_{HH} = 6.8$ Hz, 12H, $CH(CH_3)_2$), 1.01–0.98 (m, 36H, $CH(CH_3)_2$), -0.66 (s, 3H, $ZnCH_3$), -5.15 (br s, 2H, $Ru(\eta^2-H_2)$), -7.83 (br s, 1H, $RuHZn$), -12.16 (s, 1H, $RuHZn$). $^{13}C\{^1H\}$ NMR: δ_C (126 MHz, CD_2Cl_2 , 298 K, $[BAR^F_4]^{-}$ signals are omitted) 196.8 (s, RuCO), 179.6 (s, Ru_{NHC}), 146.3 (s), 145.0 (s), 137.2 (s), 131.7 (s), 126.4 (s), 126.0 (s), 125.9 (s), 29.5 (s), 29.2 (s, $CH(CH_3)_2$), 26.4 (s), 26.2 (s), 22.9 (s), 22.6 (s, $CH(CH_3)_2$), 1.38 (s, $ZnCH_3$). IR (CD_2Cl_2 , cm^{-1}): 2005 (ν_{CO}). Anal. calcd for $C_{88}H_{91}BN_4OF_{24}ZnRu \cdot CH_2Cl_2$: C, 55.13, H, 4.83, N, 2.89. Found: C, 55.6, H, 4.64, N, 2.48.

$[Ru(IPr)_2(CO)(H)_2ZnMe][BAR^F_4]^{-}$ (**9**)

A J. Young's resealable NMR tube was charged with a solution of **7** (25 mg, 0.014 mmol) in C_6H_5F (0.6 mL), degassed (freeze–pump–thaw $\times 3$) and exposed to 1 atm H_2 . After 30 min, the solvent was removed *in vacuo* and the resulting pale orange residue left under vacuum for 3 h. This was then dissolved in C_6H_5F (0.3 mL) and layered with hexane to yield orange crystals of **9**. Yield 13 mg (54%). 1H NMR: δ_H (400 MHz, CD_2Cl_2 , 298 K) 7.72 (s, 8H, $[BAR^F_4]^{-}$), 7.56 (s, 4H, $[BAR^F_4]^{-}$), 7.49 (t, $3J = 7.8$ Hz, 4H, Ar), 7.30 (d, $J = 7.8$ Hz, 4H, Ar), 7.23 (d, $J = 7.8$ Hz, 4H, Ar), 7.06 (s, 4H, NCH=NCH), 2.35 (sept, $^3J_{HH} = 6.8$ Hz, 4H, $CH(CH_3)_2$), 2.19 (sept, $^3J_{HH} = 6.8$ Hz, 4H, $CH(CH_3)_2$), 1.04–0.99 (m, 36H, $CH(CH_3)_2$), 0.44 (d, $^3J_{HH} = 6.8$ Hz, 12H, $CH(CH_3)_2$), -0.72 (s, 3H, $ZnCH_3$), -4.19 (d, $^2J = 7.7$ Hz, 1H, $RuHZn$), -25.77 (d, $^2J_{HH} = 7.7$ Hz, 1H, $RuHZn$). $^{13}C\{^1H\}$ NMR: δ_C (101 MHz, CD_2Cl_2 , 298 K, $[BAR^F_4]^{-}$ signals are omitted) 198.3 (s, RuCO), 182.2 (s, Ru_{NHC}), 146.5 (s), 144.9 (s), 136.4 (s), 131.4 (s), 126.7 (s), 125.8 (s), 125.5 (s), 29.3 (s), 29.3 (s, $CH(CH_3)_2$), 26.1 (s), 24.9 (s), 23.1 (s), 22.2 (s, $CH(CH_3)_2$), 15.7 (s, $ZnCH_3$). IR (CD_2Cl_2 , cm^{-1}): 2005 (ν_{CO}). Anal. calcd for $C_{88}H_{89}BN_4OF_{24}ZnRu$: C, 57.07, H, 4.84, N, 3.03. Found: C, 57.44, H, 4.62, N, 2.90.

$[Ru(AsPh_3)_3(CO)HCl]$ (**10**)

$[Ru(AsPh_3)_3(CO)H_2]$ (728 mg, 0.69 mmol) and IBiox6 (500 mg, 1.73 mmol) were dissolved in toluene (10 mL) and stirred in a J. Young's resealable ampoule overnight at 363 K. After addition of 53 μ L CH_2Cl_2 , stirring was continued at 383 K for a further 12 h. The solvent was removed under vacuum and the product extracted into toluene (30 mL), reduced to dryness and washed with hexane (7 mL) and EtOH (2×10 mL) to give **10** as a yellow powder. Yield 280 mg (54%). 1H NMR: δ_H (500 MHz, CD_2Cl_2 , 223 K) 4.74 (d, $J = 8.5$ Hz, 2H, CH_2O), 4.59 (q, $J = 8.4$ Hz, 4H, CH_2O), 4.51 (d, $J = 8.5$ Hz, 2H, CH_2O), 3.20–3.14 (m, 2H, Cy), 2.67–2.61 (m, 2H, Cy), 2.50–2.37 (m, 4H, Cy), 2.06–2.03 (m, 2H, Cy), 1.91–1.77 (m, 14H, Cy), 1.67–1.64 (m, 4H, Cy), 1.33–1.10 (m, 12H, Cy), -24.75 (s, 1H, RuH). $^{13}C\{^1H\}$ NMR: δ_C (126 MHz, CD_2Cl_2 , 223 K) 204.1 (s, RuCO), 164.9 (s, Ru_{NHC}), 125.3 (s), 123.8 (s, NCO), 83.9 (s), 83.2 (s, OCH_2),



65.4 (s), 64.8 (s, C_{CY}), 35.8 (s), 35.3 (s), 34.5 (s), 33.4 (s), 24.5 (s), 24.3 (s), 24.0 (s), 24.0 (s), 23.9 (s), 23.8 (s, CH_{2CY}). IR (THF, cm^{-1}): 1890 (ν_{CO}). Anal. calcd for $C_{35}H_{49}N_4O_5ClRu \cdot CH_2Cl_2 \cdot C$, 52.27; H, 6.21; N, 6.77. Found: C, 52.45; H, 6.30; N, 6.62.

[Ru(IBiox6)₂(THF)(CO)H][BAR^F₄] (11)

Na[BAR^F₄] (426 mg, 0.48 mmol) was added to a C_6H_5F solution (15 mL) of **10** (324 g, 0.44 mmol) and the suspension stirred for 12 h. After filtration, the solution was evaporated and the oily residue dissolved in THF (4 mL). Addition of hexane and vigorous stirring for 15 min afforded **11** as a yellow solid. Yield: 615 mg (85%). Crystals suitable for X-ray diffraction were obtained by slow diffusion of hexane into a concentrated C_6H_5F solution of **11** at room temperature. ¹H NMR: δ_H (500 MHz, THF-*d*₈, 298 K) 7.78 (8H, [BAR^F₄][−]), 7.57 (4H, [BAR^F₄][−]), 4.91 (d, *J* = 8.7 Hz, 2H, CH_2O), 4.88 (d, *J* = 8.7 Hz, 2H, CH_2O), 4.68 (d, *J* = 8.7 Hz, 4H, CH_2O), 2.89–2.83 (m, 2H, Cy), 2.65–2.59 (m, 2H, Cy), 2.24–2.21 (m, 2H, Cy), 2.17–2.11 (m, 4H, Cy), 2.01–1.99 (m, 2H, Cy), 1.96–1.87 (m, 10H, Cy), 1.82–1.80 (m, 4H, Cy), 1.57–1.22 (m, 14H, Cy), −26.11 (s, 1H, RuH). ¹³C{¹H} NMR: δ_C (126 MHz, THF-*d*₈, 298 K, [BAR^F₄][−] signals omitted) 205.9 (s, RuCO), 161.8 (s, RuC_{NHC}), 127.4 (s), 125.9 (s, NCO), 84.9 (s), 83.9 (s, OCH₂), 66.9 (s), 66.1 (s, C_{CY}), 37.5 (s), 36.8 (s), 36.7 (s), 35.4 (s), 26.6 (s), 25.8 (s), 25.6 (s), 24.7 (s), 24.6 (s), 24.4 (s, CH_{2CY}). IR (THF, cm^{-1}): 1929 (ν_{CO}). Anal. calcd for $C_{71}H_{69}BN_4O_6F_{24}Ru \cdot C_6H_5F$: C, 53.2; H, 4.29; N, 3.22. Found: C, 52.82; H, 4.22; N, 2.86.

[Ru(IBiox6)₂(CO)(THF)ZnMe][BAR^F₄] (12)

Addition of ZnMe₂ (67 μ L of 1.0 M in toluene, 0.067 mmol) to a J. Young's resealable NMR tube containing a C_6H_5F solution (0.6 mL) of **11** (100 mg, 0.061 mmol) resulted in an instantaneous colour change from yellow to orange. The reaction mixture was evaporated to dryness, redissolved in C_6H_5F (0.3 mL) and layered with hexane to yield orange crystals of **12**. Yield 69 mg (66%). ¹H NMR: δ_H (500 MHz, THF-*d*₈, 298 K) 7.79 (8H, [BAR^F₄][−]), 7.57 (4H, [BAR^F₄][−]), 4.78 (br s, 8H, CH_2O), 2.89 (br s, 4H, Cy), 2.71 (br s, 4H, Cy), 2.08–2.03 (m, 8H, Cy), 1.99–1.92 (m, 8H, Cy), 1.82–1.76 (m, 8H, Cy), 1.54–1.47 (m, 4H, Cy), −0.01 (s, 1H, ZnCH₃). ¹³C{¹H} NMR: δ_C (126 MHz, THF-*d*₈, 298 K, [BAR^F₄][−] signals omitted) 209.5 (s, RuCO), 161.8 (s, RuC_{NHC}), 127.5 (s, NCO), 84.2 (s, OCH₂), 68.4 (s, C_{CY}), 36.4 (s), 26.6 (s), 25.4 (s), 24.7 (s), 24.5 (s, CH_{2CY}), −0.28 (s, ZnCH₃). IR (THF, cm^{-1}): 1929 (ν_{CO}).

[Ru(IBioxMe₄)₂(CO)HCl] (13)

[Ru(AsPh₃)₃(CO)H₂] (1.11 g, 1.06 mmol) and IBioxMe₄ (552 mg, 2.65 mmol) were dissolved in toluene (10 mL) and the solution heated in a J. Young's resealable ampoule overnight at 363 K. After addition of 102 μ L (1.59 mmol) of CH_2Cl_2 , heating was continued at 393 K for a further 24 h. After that time a solid had formed, which was isolated by cannula filtration and washed with hexane (2 \times 10 mL) and EtOH (10 mL) to give **13** as a yellow powder. Yield 424 mg (69%). Yellow crystals suitable for X-ray diffraction were obtained layering a CH_2Cl_2 solution of the complex with hexane. ¹H NMR: δ_H

(500 MHz, $CDCl_3$, 298 K) 4.48 (s, 8H, CH_2O), 1.95–1.65 (s, 24H, CH_3), −25.14 (s, 1H, RuH). ¹³C{¹H} NMR: δ_C (126 MHz, $CDCl_3$, 298 K) 203.2 (s, RuCO), 166.6 (s, RuC_{NHC}), 125.4 (s), 124.5 (s, NCO), 88.0 (s), 87.4 (s, OCH₂), 61.2 (s), 60.7 (s, $C(CH_3)_2$), 27.6 (s), 27.1 (s), 26.3 (s), 26.1 (s, CH_3). IR ($CDCl_3$, cm^{-1}): 1895 (ν_{CO}). Anal. calcd for $C_{23}H_{33}N_4O_5ClRu \cdot 0.5C_6H_5F$: C, 49.56; H, 5.68; N, 8.89. Found: C, 48.97; H, 5.59; N, 8.51.

[Ru(IBioxMe₄)₂(THF)(CO)H][BAR^F₄] (14)

Na[BAR^F₄] (168 mg, 0.19 mmol) was added to a C_6H_5F solution (15 mL) of **13** (100 mg, 0.17 mmol) and the suspension stirred overnight at room temperature. After filtration, the filtrate was evaporated to dryness and the residue redissolved in THF (4 mL). Addition of hexane and vigorous stirring for 15 min afforded **14** as a brown solid. Yield 190 mg (79%). Crystals suitable for X-ray diffraction were obtained by slow diffusion of hexane into a concentrated THF solution of **14** at room temperature. ¹H NMR: δ_H (400 MHz, THF-*d*₈, 298 K) 7.80 (s, 8H, [BAR^F₄][−]), 7.59 (s, 4H, [BAR^F₄][−]), 4.71–4.66 (m, 4H, OCH₂), 4.61–4.57 (m, 4H, OCH₂), 1.90 (s, 6H, CH_3), 1.85 (s, 6H, CH_3), 1.74 (s, 6H, CH_3), 1.59 (s, 6H, CH_3), −26.13 (s, 1H, RuH). ¹³C{¹H} NMR: δ_C (101 MHz, THF, 298 K, [BAR^F₄][−] signals omitted) 203.8 (s, RuCO), 161.1 (s, RuC_{NHC}), 126.2 (s), 125.1 (s, NCO), 87.6 (s), 86.8 (s, OCH₂), 61.7 (s), 61.0 (s, $C(CH_3)_2$), 26.0 (s), 25.8 (s), 25.3 (s), 25.3 (s, CH_3). IR (THF, cm^{-1}): 1933 (ν_{CO}). Anal. calcd for $C_{55}H_{45}BF_{24}N_4O_5Ru \cdot C_4H_8O$: C, 47.82; H, 3.6; N, 3.78. Found: C, 47.89; H, 3.55; N, 3.14.

[Ru(IMes)(PPh₃)(CO)ZnMe] (15)

Rapid addition of ZnMe₂ (1.22 mL of 1.2 M solution in toluene, 1.46 mmol) to a J. Young's resealable ampoule containing a THF solution (10 mL) of [Ru(IMes)(PPh₃)(CO)HCl] (214 mg, 0.292 mmol) resulted in an instantaneous colour change from yellow to dark orange. The reaction mixture was stirred for 5 min, concentrated to ca. 1 mL and Et₂O (15 mL) added. After filtration through a short pad of Celite®, the filtrate was left to stand at room temperature, whereby an initial batch of orange crystals (94 mg, 42% yield) formed. After separation by filtration, the mother liquor was concentrated (ca. 8 mL), left to stand, and a further 40 mg of crystalline product was formed. This was shown by NMR spectroscopy to comprise of ca. 92% **15** and ca. 8% of a second product, which we assign as [Ru(IMes)(PPh₃)(CO)(ZnMe)Cl] (**16**; ESI[†]). In solution, **15** was found to exist as a mixture of two forms, believed to be the conformers **15a** and **15b**. ¹H NMR of **15a**: δ_H (400 MHz, C_6D_6 , 298 K) 7.57–7.46 (m, 6H, PPh₃), 7.06–6.94 (m, 9H, PPh₃), 6.84 (s, 1H, Ar), 6.72 (s, 1H, Ar), 6.64 (s, 1H, Ar), 6.38 (d, ³J_{HH} = 1.7 Hz, 1H, NCH=NCH), 6.21 (d, ³J_{HH} = 1.7 Hz, 1H, NCH=NCH), 6.00 (s, 1H, Ar), 3.17 (br t, ²J_{HH} = ³J_{HP} = 5.9 Hz, 1H, RuCHH), 2.27 (s, 3H, CH_3), 2.23 (s, 3H, CH_3), 2.08 (s, 6H, CH_3), 1.99 (s, 6H, CH_3), 1.59 (dd, ³J_{HP} = 11.6 Hz, ²J_{HH} = 6.5 Hz, 1H, RuCHH), −0.57 (s, 3H, ZnCH₃). ³¹P{¹H} NMR: δ_P (162 MHz, C_6D_6 , 298 K) 52.1 (s). ¹³C{¹H} NMR: δ_C (101 MHz, C_6D_6 , 298 K) 206.7 (d, ²J_{CP} = 11 Hz, RuCO), 196.2 (d, ²J_{CP} = 83 Hz, RuC_{NHC}), 139.1 (s, Ar), 138.9 (d, *J*_{CP} = 12 Hz, PPh₃), 137.5 (s, Ar), 136.6 (s, Ar), 136.3 (s, Ar), 135.2 (s, Ar), 134.4 (d, *J*_{CP} = 12.0 Hz, PPh₃), 133.1



(s, Ar), 131.6 (s, Ar), 130.5 (s, Ar), 130.2 (s, Ar), 129.1 (d, $J_{CP} = 1$ Hz, PPh₃), 128.9 (s, Ar), 128.1 (s, Ar), 125.7 (s, Ar), 122.3 (d, $^4J_{CP} = 3$ Hz, NCH=CHN), 120.3 (d, $^4J_{CP} = 3$ Hz, NCH=CHN), 31.6 (d, $^2J_{CP} = 7$ Hz, RuCH₂), 21.3 (s, CH₃), 21.1 (s, CH₃), 19.0 (s, CH₃), 18.7 (s, CH₃), 18.1 (s, CH₃), -1.5 (d, $^3J_{CP} = 3$ Hz, ZnCH₃). ¹H NMR: δ_H (500 MHz, THF-*d*₈, 298 K) 7.47–7.13 (m, 17H, Ar + NCH=CHN), 7.00 (s, 1H, Ar), 6.99 (s, 1H, Ar), 6.62 (s, 1H, Ar), 5.55 (s, 1H, Ar), 2.61 (br t, $^2J_{HH} = ^3J_{HP} = 5.6$ Hz, 1H, RuCHH), 2.34 (s, 3H, CH₃), 2.30 (s, 3H, CH₃), 2.25 (s, 3H, CH₃), 2.17 (s, 3H, CH₃), 1.87 (s, 3H, CH₃), 0.98 (dd, $^3J_{HP} = 11.6$ Hz, $^2J_{HH} = 6.7$ Hz, 1H, RuCHH), -1.21 (s, 3H, ZnCH₃). ³¹P{¹H} NMR: δ_P (202 MHz, THF-*d*₈, 298 K) 50.1 (s). Selected ¹³C{¹H} NMR: δ_C (126 MHz, THF-*d*₈, 298 K) 206.4 (d, $^2J_{CP} = 11$ Hz, RuCO), 195.9 (d, $^2J_{CP} = 83$ Hz, RuC_{NHC}), 31.1 (d, $^2J_{CP} = 7$ Hz, RuCH₂), -2.4 (d, $^3J_{CP} = 4$ Hz, ZnCH₃). **15b**: ¹H NMR: δ_H (500 MHz, THF-*d*₈, 298 K) 7.73 (s, 1H, NCH=NCH), 7.47–7.13 (m, 16 H, PPh₃ and NCH=NCH), 6.95 (s, 1H, Ar), 6.92 (s, 1H, Ar), 6.46 (s, 1H, Ar), 6.03 (s, 1H, Ar), 2.28 (s, 3H, CH₃), 2.26 (s, 3H, CH₃), 2.16 (s, 3H, CH₃), 2.12 (s, 3H, CH₃), 1.86 (s, 3H, CH₃), 1.52 (m, 1H, RuCHH), 1.40 (dd, $^3J_{HP} = 14.4$ Hz, $^2J_{HH} = 8.6$ Hz, 1H, RuCHH), -0.90 (s, 3H, ZnCH₃). ³¹P{¹H} NMR: δ_P (202 MHz, THF-*d*₈, 298 K) 57.1 (s). Selected ¹³C{¹H} NMR: δ_C (126 MHz, THF-*d*₈, 298 K) 203.3 (d, $^2J_{CP} = 8$ Hz, RuCO), 200.1 (d, $^2J_{CP} = 82$ Hz, RuC_{NHC}), 31.7 (d, $^2J_{CP} = 9$ Hz, RuCH₂), -4.0 (s, ZnCH₃). IR (KBr, cm⁻¹): 1860 (ν_{CO}). Anal. calcd for C₄₁H₄₁N₂OPRuZn: C, 63.52, H, 5.33, N, 3.61. Found: C, 63.30, H, 5.30, N, 3.69.

[Ru(IMes)(PPh₃)(CO)(H)₂ZnMe] (17)

Addition of H₂ (1 atm) to a J. Young's resealable ampoule tube containing a Et₂O solution (1 mL) of **15** (34 mg, 0.044 mmol) resulted in an instantaneous colour change from red-orange to colourless/pale yellow. After 30 min, the solvent was removed, the solid washed with Et₂O (3 × 0.5 mL) and the colourless solid dried under vacuum. Yield 19 mg (55%). ¹H NMR: δ_H (500 MHz, C₆D₆, 298 K) 7.71–7.65 (m, 6H, Ar), 7.09–6.96 (m, 9H, Ar), 6.89 (d, $^3J_{HH} = 1.3$ Hz, 1H, NCH=CHN), 6.77 (s, 1H, Ar), 6.74 (s, 1H, Ar), 6.68 (s, 1H, Ar), 6.62 (s, 1H, Ar), 6.17 (d, $^3J_{HH} = 1.4$ Hz, 1H, NCH=CHN), 3.22 (d, $^2J_{HH} = 9.2$ Hz, 1H, RuCHH), 2.26 (s, 3H, CH₃), 2.14 (s, 3H, CH₃), 2.13 (s, 3H, CH₃), 2.07 (s, 6H, CH₃), 1.83 (dd, $^3J_{HP} = 12.3$ Hz, $^2J_{HH} = 9.6$ Hz, 1H, RuCHH), -1.29 (s, 3H, ZnCH₃), -6.77 (d, $^2J_{HP} = 14.9$ Hz, 1H, RuHZn), -9.19 (d, $^2J_{HP} = 5.0$ Hz, RuHZn). ³¹P{¹H} NMR: δ_P (202 MHz, C₆D₆, 298 K) 55.4 (s). ¹³C{¹H} NMR: δ_C (126 MHz, C₆D₆, 298 K) 203.0 (d, $^2J_{CP} = 14$ Hz, RuCO), 194.6 (d, $^2J_{CP} = 83$ Hz, RuC_{NHC}), 156.0 (s, Ar), 139.9 (s, Ar), 138.7 (d, $J_{CP} = 38$ Hz, PPh₃), 137.8 (s, Ar), 137.1 (s, Ar), 136.7 (s, Ar), 135.4 (s, Ar), 135.1 (s, Ar), 134.4 (d, $J_{CP} = 11$ Hz, PPh₃), 130.8 (s, Ar), 130.5 (s, Ar), 129.4 (s, PPh₃), 128.8 (s, Ar), 125.2 (s, Ar), 121.8 (d, $^4J_{CP} = 2$ Hz, NCH=CHN), 119.5 (d, $^4J_{CP} = 3$ Hz, NCH=CHN), 21.3 (s, CH₃), 21.1 (s, CH₃), 19.8 (s, CH₃), 18.7 (s, CH₃), 18.4 (s, CH₃), 7.7 (d, $^2J_{CP} = 7$ Hz, RuCH₂), -5.4 (s, ZnCH₃). IR (KBr, cm⁻¹): 1941 (ν_{CO}). Efforts to record elemental analyses repeatedly gave low %C values (e.g. Anal. calcd for C₄₁H₄₃N₂OPRuZn: C, 63.36, H, 5.58, N, 3.60. Found: C, 61.23, H, 5.40, N, 3.65) which we attribute to the decomposition of the compound with time.

X-ray crystallography

Data for **7**, **9**, **11** and **12** were collected using an Agilent Xcalibur diffractometer while those for **8**, **10**, **13**, **14**, **15** and **17** were obtained using an Agilent SuperNova instrument (Table 2). All experiments were conducted at 150 K, solved using charge-flipping algorithm implemented in Olex2²⁴ and refined using SHELXL.²⁵ In structures where disorder was observed in a [BAR^F₄] anion, C–F, F...F, C...F and ADP restraints were applied, on merit. Otherwise, refinements were largely straightforward. Hence, only points of merit will be detailed hereafter. The asymmetric unit in **7** comprises one cation and one anion. The hydrogens attached to C55 in the former were located and refined subject to having similar C–H bond distances and to being equidistant from each other. F7, F8 and F9 were each disordered over 2 sites in the anion. H1, H2 and H3 in the cationic portion of compound **8** were readily located and, after some effort, an assignment was also made for H4. The associated *U*_{iso} values were refined freely, and that for H4 is somewhat higher than one might expect. However, this may well reflect some movement in the ligated dihydrogen, wherein the constituent atoms were refined subject to being equidistant from Ru1 and at a distance of 0.75 Å from each other (the refined H–H distance, on this basis, is 0.75(1) Å). The bridging hydrides were refined without restraints. Residual electron density maxima in this structure are in the region of the anion CF₃ groups, five of which merited disorder modelling. In particular, F7–F12 were each refined over 2 positions in a 50 : 50 disorder ratio while F1–F3 exhibited 70 : 30 disorder. Moreover, the entire CF₃ moieties based on C71 and C80 were refined to take account of 70 : 30 and 55 : 45 disorder levels, respectively.

In **9**, the asymmetric unit contains one cation, one anion and one molecule of CH₂Cl₂. H1 and H2 in the cation were located a refined without restraints. The hydrogens attached to C26 were similarly located and refined subject to being located at a distance of 0.98 Å from C26. Fluoride disorder was modelled for two of the [BAR^F₄] CF₃ moieties. In particular, F1–F3 were disordered over two sites in a 75 : 25 ratio while F13–15 were disordered over three sites in a 50 : 40 : 10 ratio. The solvent molecule exhibited 55 : 45 disorder and C–Cl distances were restrained to being similar in both moieties. ADP restraints were included for fractional occupancy atoms. The asymmetric unit in **10** equates to half of one molecule of the complex, and half of a benzene molecule. The chloride and carbonyl ligands within the metal complex are disordered with each other in a 50 : 50 ratio. The hydride ligand (which is likely to be disordered over 2 sites) could not be reliably located and, hence, was omitted from the refinement. One cation, one anion and two independent fluorobenzene halves constitute the asymmetric unit in **11**. The solvent moieties are proximate to crystallographic inversion centres which serve, in each case, to generate the remaining molecule portions. The halides in these solvent moieties are necessarily disordered and, hence, exhibit half site-occupancies. 75 : 25 disorder was also modelled for C22 in the cation, with chemically similar distances





Table 2 Crystal data and structure refinement details for compounds 7–15 and 17

Identification code	7	8	9	10	11
Empirical formula	C ₈₈ H ₈₇ BF ₂₄ N ₄ ORuZn	C ₈₈ H ₉₁ BF ₂₄ N ₄ ORuZn	C ₈₉ H ₉₁ BCl ₂ F ₂₄ N ₄ ORuZn	C ₄₁ H ₅₅ ClN ₄ O ₅ Ru	C ₇₇ H ₇₄ BF ₂₅ N ₄ O ₆ Ru
Formula weight	1849.86	1853.89	1936.80	820.41	1738.28
Crystal system	Orthorhombic	Triclinic	Triclinic	Monoclinic	Triclinic
Space group	<i>P</i> 2 ₁ 2 ₁ 2 ₁	<i>P</i> $\bar{1}$	<i>P</i> $\bar{1}$	<i>C</i> 2/ <i>c</i>	<i>P</i> $\bar{1}$
<i>a</i> /Å	16.4346(4)	12.7837(2)	13.1638(4)	22.2537(14)	14.9600(4)
<i>b</i> /Å	21.1397(5)	17.1267(3)	17.7078(6)	13.5448(8)	15.8674(5)
<i>c</i> /Å	24.5462(5)	20.4172(3)	19.6253(6)	12.4203(7)	16.5741(5)
α /°	90	84.063(1)	95.885(2)	90	87.261(3)
β /°	90	88.767(1)	94.337(2)	93.810(5)	80.381(2)
γ /°	90	85.402(1)	98.208(2)	90	75.276(2)
<i>U</i> /Å ³	8527.9(3)	4431.51(12)	4485.0(2)	3735.5(4)	3751.5(2)
<i>Z</i>	4	2	2	4	2
ρ_{calc} /g cm ⁻³	1.441	1.389	1.434	1.459	1.539
μ /mm ⁻¹	0.559	0.538	0.593	4.463	0.327
<i>F</i> (000)	3784.0	1900.0	1980.0	1720.0	1772.0
Crystal size/mm ³	0.528 × 0.38 × 0.378	0.317 × 0.132 × 0.103	0.577 × 0.493 × 0.41	0.324 × 0.214 × 0.167	0.56 × 0.542 × 0.434
Radiation	MoK α	MoK α	MoK α	CuK α	MoK α
2 θ range for data collection/°	6.668 to 54.968	5.164 to 61.016	6.794 to 54.968	10.28 to 145.568	6.87 to 54.968
Index ranges	–20 ≤ <i>h</i> ≤ 18 –27 ≤ <i>k</i> ≤ 27 –31 ≤ <i>l</i> ≤ 31	–18 ≤ <i>h</i> ≤ 18 –24 ≤ <i>k</i> ≤ 24 –29 ≤ <i>l</i> ≤ 28	–17 ≤ <i>h</i> ≤ 17 –22 ≤ <i>k</i> ≤ 19 –24 ≤ <i>l</i> ≤ 22	–26 ≤ <i>h</i> ≤ 27 –16 ≤ <i>k</i> ≤ 16 –15 ≤ <i>l</i> ≤ 9	–17 ≤ <i>h</i> ≤ 19 –18 ≤ <i>k</i> ≤ 20 –21 ≤ <i>l</i> ≤ 21
Reflections collected	77 177	159 961	40 172	16 638	46 082
Independent reflections, <i>R</i> _{int}	19 171, 0.0429	26 703, 0.0629	19 792, 0.0362	3649, 0.0935	16 803, 0.0392
Data/restraints/parameters	19 171/67/1136	26 703/157/1267	19 792/240/1246	3649/0/249	16 803/334/1188
Goodness-of-fit on <i>F</i> ²	1.077	1.042	1.037	1.074	1.063
Final <i>R</i> ₁ , w <i>R</i> ₂ , <i>I</i> ≥ 2 σ (<i>I</i>)	0.0511, 0.1112	0.0503, 0.1188	0.0467, 0.1017	0.0512, 0.1314	0.0617, 0.1407
Final <i>R</i> ₁ , w <i>R</i> ₂ , all data	0.0680, 0.1206	0.0694, 0.1298	0.0675, 0.1136	0.0531, 0.1326	0.0813, 0.1516
Largest diff. peak/hole/e Å ⁻³	0.83/–0.86	0.76/–1.18	0.88/–0.57	0.68/–0.64	2.80/–0.68
Flack parameter	0.017(4)	—	—	—	—

Identification code	12	13	14	15	17
Empirical formula	C ₇₂ H ₇₁ BF ₂₄ N ₄ O ₆ RuZn	C ₂₃ H ₃₂ ClN ₄ O ₅ Ru	C ₅₉ H ₅₂ BF ₂₄ N ₄ O ₆ Ru	C ₄₁ H ₄₁ N ₂ OPRuZn	C ₄₁ H ₄₃ N ₂ OPRuZn
Formula weight	1721.57	581.04	1480.92	775.17	777.18
Crystal system	Triclinic	Monoclinic	Triclinic	Monoclinic	Triclinic
Space group	<i>P</i> $\bar{1}$	<i>P</i> 2 ₁ / <i>n</i>	<i>P</i> $\bar{1}$	<i>P</i> 2 ₁ / <i>c</i>	<i>P</i> $\bar{1}$
<i>a</i> /Å	12.9608(4)	10.2772(2)	9.9024(1)	10.5880(1)	9.8428(2)
<i>b</i> /Å	13.1449(4)	11.4391(2)	18.4531(2)	25.6243(2)	11.4984(3)
<i>c</i> /Å	21.6148(7)	10.8292(2)	19.4882(3)	13.6538(1)	17.9210(3)
α /°	94.981(3)	90	112.078(1)	90	87.163(2)
β /°	91.296(3)	99.331(2)	103.002(1)	103.780(1)	81.171(2)
γ /°	97.163(3)	90	96.389(1)	90	65.917(2)
<i>U</i> /Å ³	3637.8(2)	1256.26(4)	3138.80(7)	3597.79(5)	1829.55(7)
<i>Z</i>	2	2	2	4	2
ρ_{calc} /g cm ⁻³	1.572	1.536	1.567	1.431	1.411
μ /mm ⁻¹	0.654	6.375	3.144	4.896	4.814
<i>F</i> (000)	1748.0	598.0	1494.0	1592.0	800.0
Crystal size/mm ³	0.561 × 0.375 × 0.27	0.072 × 0.058 × 0.019	0.283 × 0.229 × 0.094	0.471 × 0.095 × 0.092	0.116 × 0.08 × 0.05
Radiation	MoK α	CuK α	CuK α	CuK α	CuK α
2 θ range for data collection/°	6.678 to 54.966	11.012 to 146.588	5.636 to 147.162	6.9 to 146.304	4.99 to 146.094

Table 2 (Contd.)

Identification code	12	13	14	15	17
Index ranges	-16 ≤ h ≤ 16 -17 ≤ k ≤ 16 -27 ≤ l ≤ 28	-12 ≤ h ≤ 12 -14 ≤ k ≤ 11 -11 ≤ l ≤ 13	-9 ≤ h ≤ 12 -22 ≤ k ≤ 22 -24 ≤ l ≤ 24	-13 ≤ h ≤ 9 -31 ≤ k ≤ 31 -16 ≤ l ≤ 16	-12 ≤ h ≤ 12 -14 ≤ k ≤ 14 -20 ≤ l ≤ 22
Reflections collected	33 375	13 001	62 311	47 648	21 138
Independent reflections, R_{int}	16 641, 0.0262	2531, 0.0392	12 599, 0.0418	7195, 0.0440	7307, 0.0340
Data/restraints/parameters	16 641/264/1097	2531/0/173	12 599/2804/1493	7195/2/438	7307/2/446
Goodness-of-fit on F^2	1.027	1.194	1.039	1.056	1.020
Final R_1 , wR_2 , $I \geq 2\sigma(I)$	0.0441, 0.1015	0.0343, 0.0721	0.0530, 0.1471	0.0279, 0.0729	0.0274, 0.0650
Final R_1 , wR_2 , all data	0.0580, 0.1096	0.0378, 0.0736	0.0573, 0.1523	0.0294, 0.0740	0.0311, 0.0672
Largest diff. peak/hole/ $e \text{ \AA}^{-3}$	0.98/-0.65	0.50/-0.55	1.46/-1.04	1.02/-0.62	0.61/-0.52

in each disordered component being restrained to being similar. The hydride was also located and is disordered in a 50 : 50 ratio. The associated metal-hydride distances were refined subject to a 1.6 Å, Ru–H, distance restraint. Anion disorder was limited to the halides in five of the CF₃ functionalities. Specifically, the fluorines attached to C46, C54, C55, C63 and C70 exhibited disorder ratios of 65 : 35, 55 : 45, 50 : 50, 75 : 25 and 75 : 25, respectively.

Some disorder modelling was necessary in both that cation and the anion present in the asymmetric unit of compound **12**. In the cation, this pertained to 55 : 45 disorder confined to atoms C37 and C38 in the THF ligand. Chemically equivalent distances involving the partial occupancy atoms were restrained to being similar in the final least-squares and some ADP restraints were also included for same. Four of the CF₃ groups in the anion were seen to exhibit disorder. In particular, the fluorine atoms attached to C47, C56, C63 and C72 were each modelled over 2 sites, in ratios of 55 : 45, 60 : 40, 55 : 45 and 75 : 25, respectively. The asymmetric unit in **13** comprises half of a molecule, with the central ruthenium located at a crystallographic inversion centre. This necessarily means that the chloride and carbonyl ligands are disordered in a 50 : 50 ratio. An exemplary diffraction pattern was observed for crystal of compound **14** where the asymmetric unit was seen to contain one cation and one anion. There was no evident twinning but, yet, the structural motif itself is riddled with disorder. While this was successfully modelled, it has inevitably resulted in the addition of a large number of restraints to the model, as both carbene ligands in the cation were seen to be disordered in a 50 : 50 ratio. The carbene carbons are, in each ligand, common to both components. In addition, C26 in the THF ligand was also seen to exhibit disorder, which optimally refined to a 60 : 40 ratio. Distance similarity restraints and ADP restraints were added to the model for the cation, on merit, in the final refinement cycles. In the BAR^F₄ anion, three of the rings were seen to be disordered in an 80 : 20 ratio. The moiety based on C36 did not exhibit disorder to a level that could be credibly modelled, although the CF₃ group based on C42 was treated for 70 : 30 disorder.

In **15**, both H3a and H3b were located and subsequently refined subject to each being a distance of 0.98 Å from C3. In a similar vein, the hydrogens attached to C3 were also readily located in **17**, and each refined subject to being situated at distance of 0.95 Å from the parent atom. Finally, the bridging hydride ligands were also located in this compound and refined without restraints.

Crystallographic data for all compounds have been deposited with the Cambridge Crystallographic Data Centre as supplementary publications CCDC 1882150 (compound **7**), 1882152 (**8**), 1882151 (**9**), 1882153 (**10**), 1882154 (**11**), 1882155 (**12**), 1882156 (**13**), 1882157 (**14**), 1882158 (**15**) and 1882159 (**17**).†

Conflicts of interest

There are no conflicts of interest to declare.



Acknowledgements

We thank the EU (Marie Curie Individual Fellowships to ME-V (700189 H2020-MSCA-IF 2015) and FMM (792674 H2020-MSCA-IF 2017)) and EPSRC (grant EP/J009962/1; IMR) for financial support. VV-I thanks MINECO/FEDER (CTQ2017-83421-P) and Gobierno de Aragón (GA/FEDER, Inorganic Molecular Architecture Group E08_17R) for financial support and MINECO/FEDER for a FPI fellowship. We thank Dr Adrian Chaplin for an initial gift of IBiox6 and for subsequent assistance in the syntheses of the IBiox ligands. We are delighted to dedicate this paper to Professor Geoff Cloke FRS on the occasion of his 65th birthday.

References

- 1 A. Maity and T. S. Teets, *Chem. Rev.*, 2016, **116**, 8873–8911.
- 2 (a) W. H. Harman and J. C. Peters, *J. Am. Chem. Soc.*, 2012, **134**, 5080–5082; (b) W. H. Harman, T.-P. Lin and J. C. Peters, *Angew. Chem., Int. Ed.*, 2014, **53**, 1081–1086; (c) B. R. Barnett, C. E. Moore, A. L. Rheingold and J. S. Figueroa, *J. Am. Chem. Soc.*, 2014, **136**, 10262–10265; (d) M. A. Nesbit, D. L. M. Suess and J. C. Peters, *Organometallics*, 2015, **34**, 4741–4752; (e) S. N. MacMillan, W. H. Harman and J. C. Peters, *Chem. Sci.*, 2014, **5**, 590–597; (f) M. Devillard, G. Bouhadir and D. Bourissou, *Angew. Chem., Int. Ed.*, 2015, **54**, 730–732; (g) G. Bouhadir and D. Bourissou, *Chem. Soc. Rev.*, 2016, **45**, 1065–1079; (h) K. N. T. Tseng, J. W. Kampf and N. K. Szymczak, *J. Am. Chem. Soc.*, 2016, **138**, 10378–10381; (i) M. Devillard, R. Declercq, E. Nicolas, A. W. Ehlers, J. Backs, N. Saffon-Merceron, G. Bouhadir, J. C. Slootweg, W. Uhl and D. Bourissou, *J. Am. Chem. Soc.*, 2016, **138**, 4917–4926; (j) G. R. Owen, *Chem. Commun.*, 2016, **52**, 10712–10726; (k) J. Takaya and N. Iwasawa, *J. Am. Chem. Soc.*, 2017, **139**, 6074–6077.
- 3 J. A. B. Abdalla and S. Aldridge, in *Molecular Metal-Metal Bonds: Compounds, Synthesis, Properties*, ed. S. T. Liddle, Wiley-VCH, Weinheim, 2015, pp. 455–484.
- 4 (a) F. N. Tebbe, *J. Am. Chem. Soc.*, 1973, **95**, 5412–5414; (b) J. N. St. Denis, W. Butler, M. D. Glick and J. P. Oliver, *J. Organomet. Chem.*, 1977, **129**, 1–16; (c) P. H. M. Budzelaar, K. H. Denhaan, J. Boersma, G. J. M. Vanderkerk and A. L. Spek, *Organometallics*, 1984, **3**, 156–159; (d) P. H. M. Budzelaar, A. A. H. Vanderzeijden, J. Boersma, G. J. M. Vanderkerk, A. L. Spek and A. J. M. Duisenberg, *Organometallics*, 1984, **3**, 159–163; (e) W. A. Skupiński, J. C. Huffman, J. W. Bruno and K. G. Caulton, *J. Am. Chem. Soc.*, 1984, **106**, 8128–8136; (f) D. L. Thorn and R. L. Harlow, *J. Am. Chem. Soc.*, 1989, **111**, 2575–2580; (g) M. D. Fryzuk, D. H. McConville and S. J. Rettig, *Organometallics*, 1990, **9**, 1359–1360; (h) M. D. Fryzuk, D. H. McConville and S. J. Rettig, *Organometallics*, 1993, **12**, 2152–2161; (i) J. T. Golden, T. H. Peterson, P. L. Holland, R. G. Bergman and R. A. Andersen, *J. Am. Chem. Soc.*, 1998, **120**, 223–224; (j) C. J. Durango-García, J. O. C. Jiménez-Halla, M. López-Cardoso, V. Montiel-Palma, M. A. Muñoz-Hernández and G. Merino, *Dalton Trans.*, 2010, **39**, 10588–10589.
- 5 I. M. Riddlestone, D. McKay, M. J. Gutmann, S. A. Macgregor, M. F. Mahon, H. A. Sparkes and M. K. Whittlesey, *Organometallics*, 2016, **35**, 1301–1312.
- 6 (a) I. M. Riddlestone, N. A. Rajabi, S. A. Macgregor, M. F. Mahon and M. K. Whittlesey, *Chem. – Eur. J.*, 2018, **24**, 1732–1738; (b) I. M. Riddlestone, N. A. Rajabi, J. P. Lowe, M. F. Mahon, S. A. Macgregor and M. K. Whittlesey, *J. Am. Chem. Soc.*, 2016, **138**, 11081–11084.
- 7 For a review that includes discussion of transition metal-H-Zn species, see: M. J. Butler and M. R. Crimmin, *Chem. Commun.*, 2017, **53**, 1348–1365.
- 8 For other examples of Ru-H-Zn complexes, see: (a) M. Molon, C. Gemel and R. A. Fischer, *Eur. J. Inorg. Chem.*, 2013, 3616–3622; (b) M. Plois, W. Hujo, S. Grimme, C. Schwickert, E. Bill, B. de Bruin, R. Pöttgen and R. Wolf, *Angew. Chem., Int. Ed.*, 2013, **52**, 1314–1318; (c) M. Plois, R. Wolf, W. Hujo and S. Grimme, *Eur. J. Inorg. Chem.*, 2013, 3039–3048; (d) S. Lau, A. J. P. White, I. J. Casely and M. R. Crimmin, *Organometallics*, 2018, **37**, 4521–4526.
- 9 J. P. Lee, Z. L. Ke, M. A. Ramírez, T. B. Gunnoe, T. R. Cundari, P. D. Boyle and J. L. Petersen, *Organometallics*, 2009, **28**, 1758–1775.
- 10 For a review of Ru-Zn containing complexes, see: T. Bollermann, C. Gemel and R. A. Fischer, *Coord. Chem. Rev.*, 2012, **256**, 537–555.
- 11 As the nature of the hydrides in the {Ru(H)₂Zn} moiety is ambiguous, we did not adopt the half-arrow formalism of Parkin. J. C. Green, M. L. H. Green and G. Parkin, *Chem. Commun.*, 2012, **48**, 11841–11503.
- 12 (a) G. Altenhoff, R. Goddard, C. W. Lehmann and F. Glorius, *Angew. Chem., Int. Ed.*, 2003, **42**, 3690–3693; (b) G. Altenhoff, R. Goddard, C. W. Lehmann and F. Glorius, *J. Am. Chem. Soc.*, 2004, **126**, 15195–15201.
- 13 (a) A. B. Chaplin, *Organometallics*, 2014, **33**, 3069–3077; (b) A. B. Chaplin, *Organometallics*, 2014, **33**, 624–626; (c) J. N. Luy, S. A. Hauser, A. B. Chaplin and R. Tonner, *Organometallics*, 2015, **34**, 5099–5112; (d) S. A. Hauser, R. Tonner and A. B. Chaplin, *Organometallics*, 2015, **34**, 4419–4427; (e) J.-N. Luy, S. A. Hauser, A. B. Chaplin and R. Tonner, *Organometallics*, 2016, **34**, 5099–5112.
- 14 K. Vehlou, M. Porta and S. Blechert, *ChemCatChem*, 2010, **2**, 803–806.
- 15 V. L. Chantler, S. L. Chatwin, R. F. R. Jazzar, M. F. Mahon, O. Saker and M. K. Whittlesey, *Dalton Trans.*, 2008, 2603–2614.
- 16 (a) S. L. Chatwin, M. G. Davidson, C. Doherty, S. M. Donald, R. F. R. Jazzar, S. A. Macgregor, G. J. McIntyre, M. F. Mahon and M. K. Whittlesey, *Organometallics*, 2006, **25**, 99–110; (b) T. E. Wang, C. Pranckevicius, C. L. Lund, M. J. Sgro and D. W. Stephan, *Organometallics*, 2013, **32**, 2168–2177; (c) C. Pranckevicius,



- L. Fan and D. W. Stephan, *J. Am. Chem. Soc.*, 2015, **137**, 5582–5589.
- 17 D. Huang, J. C. Bollinger, W. E. Streib, K. Folting, J. V. Young, O. Eisenstein and K. G. Caulton, *Organometallics*, 2000, **19**, 2281–2290.
- 18 NHC centroids were calculated from the central five-membered IBiox ring containing the coordinated carbenic carbon, the two nitrogen atoms and the two backbone carbons.
- 19 Addition of excess ZnMe_2 (or ZnEt_2) to **14** in $\text{C}_6\text{H}_5\text{F}$ resulted in complete loss of the hydride resonance of the starting material and a change in the colour of the solution from orange to purple. However, within a few minutes, the solution turned black. Nothing conclusive could be extracted from analysis of the ^1H NMR spectrum and efforts to identify products by crystallisation proved unsuccessful.
- 20 (a) R. F. R. Jazzar, S. A. Macgregor, M. F. Mahon, S. P. Richards and M. K. Whittlesey, *J. Am. Chem. Soc.*, 2002, **124**, 4944–4945; (b) T. M. Trnka, J. P. Morgan, M. S. Sanford, T. E. Wilhelm, M. Scholl, T. L. Choi, S. Ding, M. W. Day and R. H. Grubbs, *J. Am. Chem. Soc.*, 2003, **125**, 2546–2558; (c) K. Abdur-Rashid, T. Fedorkiw, A. J. Lough and R. H. Morris, *Organometallics*, 2004, **23**, 86–94; (d) S. P. Reade, A. L. Acton, M. F. Mahon, T. A. Martin and M. K. Whittlesey, *Eur. J. Inorg. Chem.*, 2009, 1774–1785; (e) H. J. Liu, M. S. Ziegler and T. D. Tilley, *Polyhedron*, 2014, **84**, 203–208; (f) H. J. Liu, M. S. Ziegler and T. D. Tilley, *Dalton Trans.*, 2018, **47**, 12138–12146.
- 21 (a) S. H. Hong, A. G. Wenzel, T. T. Salguero, M. W. Day and R. H. Grubbs, *J. Am. Chem. Soc.*, 2007, **129**, 7961–7968; (b) G. A. Bailey, J. A. M. Lummiss, M. Foscatto, G. Occhipinti, R. McDonald, V. R. Jensen and D. E. Fogg, *J. Am. Chem. Soc.*, 2017, **139**, 16446–16449.
- 22 Unsurprisingly, the reverse reaction ($\text{17-d}_2 + \text{H}_2$) gave **17**.
- 23 U. L. Dharmasena, H. M. Foucault, E. N. dos Santos, D. E. Fogg and S. P. Nolan, *Organometallics*, 2005, **24**, 1056–1058.
- 24 O. V. Dolomanov, L. J. Bourhis, R. J. Gildea, J. A. K. Howard and H. Puschmann, *J. Appl. Crystallogr.*, 2009, **42**, 339–341.
- 25 G. M. Sheldrick, *Acta Crystallogr., Sect. A: Found. Crystallogr.*, 1990, **A46**, 467–473; G. M. Sheldrick, *SHELXL-97, a computer program for crystal structure refinement*, University of Göttingen, 1997.

